Ludden, J.N., Plank, T., and Escutia, C. (Eds.)
Proceedings of the Ocean Drilling Program, Scientific Results Volume 185

12. Data Report: Electrical Resistivity and X-Ray Computed Tomography Measurements of Sedimentary and Igneous Units from Hole 801C and Site 1149[1]

Tetsuro Hirono[2] and Lewis J. Abrams[3]

ABSTRACT

The results of shore-based three-axis resistivity and X-ray computed tomography (CT) measurements on cube-shaped samples recovered during Leg 185 are presented along with moisture and density, *P*-wave velocity, resistivity, and X-ray CT measurements on whole-round samples of representative lithologies from Site 1149. These measurements augment the standard suite of physical properties obtained during Leg 185 from the cube samples and samples obtained adjacent to the cut cubes. Both shipboard and shore-based measurements of physical properties provide information that assists in characterizing lithologic units, correlating cored material with downhole logging data, understanding the nature of consolidation, and interpreting seismic reflection profiles.

INTRODUCTION

The majority of samples for this study are from the world's oldest (~170 Ma) in situ oceanic crust cored in Hole 801C. The physical properties of these primary crystalline rocks removed from depth and measured at atmospheric pressures are strongly related to both the original porosity and secondary porosity because of stress unloading and the coring process. Alteration products, infilling of fractures and voids with

[1] Hirono, T., and Abrams, L.J., 2002. Data report: Electrical resistivity and X-ray computed tomography measurements of sedimentary and igneous units from Hole 801C and Site 1149. *In* Ludden, J.N., Plank, T., and Escutia, C. (Eds.), *Proc. ODP, Sci. Results,* 185, 1–18 [Online]. Available from World Wide Web: <http://www-odp.tamu.edu/publications/185_SR/VOLUME/CHAPTERS/005.PDF>. [Cited YYYY-MM-DD]
[2] Interactive Research Center of Science, Tokyo Institute of Technology, Tokyo 152-8551, Japan. t-hirono@spa.att.ne.jp
[3] University of North Carolina, Center for Marine Science, One Marvin Moss Lane, Wilmington NC 28409, USA.

Initial receipt: 18 October 2001
Acceptance: 17 May 2002
Web publication: 23 October 2002
Ms 185SR-005

secondary phases, and contributions from sediment also influence the physical state of the recovered oceanic crust. Thus, physical properties measurements are indicators of lithologic type, texture, and degree of alteration and are used to assess the physical state of the oceanic crust with depth and to establish the correlation between downhole measurements and cored material. The results of shore-based measurements of resistivity and X-ray computer tomography (CT) of over 100 discrete cube-shaped samples from Hole 801C and Site 1149 are presented in Tables T1 and T2, respectively. Resistivity measurements on cored samples are particularly useful for a number of reasons; it is a measurement that is also obtained from the borehole wall by downhole instruments, and it is strongly dependent on porosity, type and amount of pore fluid present, and pore structure geometry. These attributes are, in turn, the most important variables controlling density and velocity in the basalts cored in Hole 801C. Evaluation of physical properties measurements to assess the physical state of oceanic crust are presented in R.D. Jarrard, L.J. Abrams, R. Pockalny, R.L. Larson, and T. Hirono (unpubl. data) and Hirono (this volume).

X-ray CT measurements of discrete samples of oceanic crust, sediments, and sedimentary rocks were obtained to image in a nondestructive measurement of internal structures in an attempt to further quantify pore geometry. It was hoped that these images would provide constraints for permeability measurements (Hirono, this volume); however, pore geometry was not resolvable using this technique.

T1. Wet and dry resistivity and average Nct of cube samples, p. 15.

T2. Wet and dry resistivity along three orthogonal directions of cube samples, p. 17.

DESCRIPTION OF SAMPLING

Cube-Shaped Samples

During Leg 185, igneous and sedimentary rocks were sawed as oriented cubes (~2.2 × ~2.2 × ~2.2 cm sides), and velocities were measured in three mutually perpendicular directions (x, y, and z). Standard moisture and density, including density and porosity, were measured on the smaller volume fragments adjacent to the cut cube (Fig. F1). One sample per section (every 1.5 m) was generally taken in cores from Hole 801C, making this one of the best sampled in situ crustal sections (Shipboard Scientific Party, 2000a). Six cube samples were taken of representative lithologies from Hole 1149B (Table T2). These sample cubes were then used for shore-based measurements of electrical resistivity and for X-ray CT imaging, which is presented in this data report.

F1. Schematic diagram for sampling, p. 7.

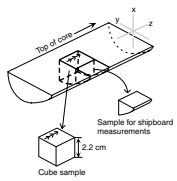

Whole-Round Samples

During Leg 185, whole-round samples of representative sediments and rocks from Site 1149 were taken and immediately sealed in bags for subsequent shore-based permeability experiments (Hirono, this volume). X-ray CT measurements of these samples were obtained in an unsuccessful attempt to quantify the pore structures as a reference for permeability measurements (Hirono, this volume). Shore-based measurements of X-ray CT, velocity, and moisture and density on these samples are presented in Table T3.

T3. Moisture and density, resistivity, and average Nct of whole-round core samples, p. 18.

ELECTRICAL RESISTIVITY

Electrical resistivity was measured on the cube-shaped samples by the simple apparatus shown in Figure **F2.** Two cells contain a conductive medium of agar-agar with KCl. Samples were placed tightly in the central support member between these cells, and measurements were taken along three orthogonal directions (Fig. **F1**). The electric current was measured at constant voltage. Resistivity (ρ [Ωm]) can be calculated using Ohm's law after correction for the length (L [Ωm]) and contact area (S = m²) of each sample as follows:

$$R = (L/S)\rho$$

where R is electric resistance (in Ω). Measurements are accurate to within 10%. Samples were first oven dried at 105°C for 24 hr and allowed to cool in a desiccator. Resistivity measurements were then obtained (dry resistivity). Resistivity was again determined after samples were soaked in distilled water for 24 hr (wet resistivity). All the data are shown in Tables **T1** and **T2.** Ten of the cube samples had resistivities too high to measure using our equipment (i.e., >9999.9 Ωm). Wet resistivities of whole-round cores were also measured along the vertical (z) direction (Table **T3**).

Wet resistivity data are compared to downhole measurements of resistivity obtained with the Dual Laterolog (Fig. **F3**). Hydrothermal deposits and interpillow material show the highest resistivity anisotropy, and the resistivities of discrete samples are generally higher than those of downhole logging, although they show similar trends. This difference is primarily because of downhole logging sensitivity to larger-scale porosity.

F2. Equipment used for measuring electrical resistivity, p. 8.

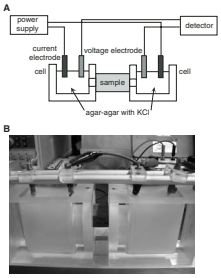

X-RAY CT

X-ray CT is a radiological imaging system first developed by Hounsfield (1973). The attenuation of two-dimensional fan beams of X-rays that penetrate a sample is measured by an array of detectors. These X-ray projection data from various directions are obtained by stacking contiguous two-dimensional images (Fig. **F4**). The degree of X-ray attenuation depends on the density and atomic number of atoms composing the samples. Higher density and higher atomic numbers result in higher attenuation of X-rays.

An X-ray CT scanner (W2000) at the Geological Survey of Japan (Hitachi Medical Co., Tokyo, Japan) was used in the present study (Fig. **F4A**). A target (Mo-W alloy) in an X-ray tube produces X-rays by collision with electrons accelerated at 120 kV with a 150-mA current. X-rays that have penetrated the sample are measured by 768 detectors. The in-plane resolution (voxel size) of the X-ray CT is 0.31 mm. The X-ray CT reports the data in the form of the so-called CT number (Nct) defined as

$$\mathrm{Nct} = (N - \mathrm{Nw})/\mathrm{Nw} \times 1000,$$

where N is the linear X-ray absorption coefficient of the sample and Nw is the linear absorption coefficient of the standard reference, pure water. The Nct of water appears with a value of 0 and that of a nonattenuating

F3. Wet resistivities along three mutually perpendicular directions of cube samples, p. 9.

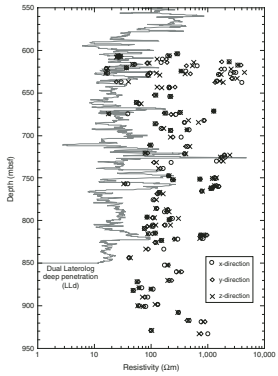

F4. Medical X-ray CT scanner, p. 10.

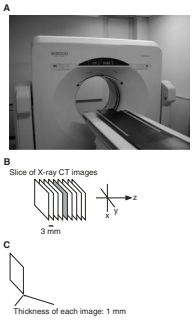

material, such as air, appears with a value of –1000. The Nct is a function of the density, state, and chemical composition of the material in any voxel.

The typical imaging parameters used are as follows:

Reconstruction filter = 6.
X-ray tube current = 120 mA (cube samples) or 100 mA (whole rounds).
Voltage = 150 kV (cube samples) or 120 kV (whole rounds).
Slice thickness = 1.0 mm (thickness of the X-ray fan beam).
Voxel size = 0.313 × 0.313 × 1.0 mm³.
Scan time = 4.0 s.
Imaging diameter = 160 mm.
Pixel matrix size = 512 × 512.

In addition, T.B.C. compensation (a compensation filter) is applied to remove the high-attenuation artifact that generally appears in CT images from the outer rim of a sample.

The output CT images are digitized as TIFF formatted, 16-bit, gray-scale image files. The original data are converted to 8-bit color images because the operating systems of popular personal computers such as Macintosh and PC cannot generally support 16-bit images. The converted 256-color values (8 bit) are linearly interpolated over a range of Ncts from 0 to 4000. Each color grade in an X-ray CT image consequently represents a 15.625-Nct range (e.g., Fig. **F5**).

A series of eight slice images was obtained from each cube sample. The space between each slice is 3 mm (Fig. **F4B**), and each slice has a 1-mm thickness (Fig. **F4C**). For the whole-round cores, there is no space between each slice and each slice has a 1-mm thickness (Fig. **F6A**). The image from the middle slice (Fig. **F4B**) on both cubes and whole-round samples was used for the calculation of the average Nct. Because one slice image has 60 pixels × 60 pixels, the average is from 3600 Nct. The results are presented in Tables **T1, T2,** and **T3.**

Processed CT images from whole-round core samples of representative lithologies are shown in Fig. **F5.** Lamination can be observed in the radiolarian porcellanite and chert and nannofossil chalk samples. The high attenuation of X-rays (red) displayed in Figure **F5G** appears to be associated with a relatively altered portion of the sample. Although altered basalt has a lower density than fresh basalt, the relatively high Nct indicates the presence of atoms of a high atomic number. We speculate that this is due to absorption of heavy metals (e.g., Zn) onto the surface of clay minerals.

Three-dimensional X-ray attenuation distribution can be reconstructed using a series of slice images (Fig. **F4B**). An example of such a reconstructed image is shown in Figure **F6A,** and a cross-sectional image perpendicular to coring direction (z-vertical) is shown in Figure **F6B.** X-ray CT images of selected cube samples are shown in Fig. **F7.**

The relationships between the average Nct from basalt cube samples and shipboard wet bulk density values (Shipboard Scientific Party, 2000a; see Table T11, p. 204, in the "Site 801" chapter) are shown in Figure **F8.** Samples with higher density generally correlate with higher Nct samples (R = 0.89), as expected. There are some exceptions such as basalt Sample 185-801C-33R-1, 11–13 cm, which has a relatively low density (2.49 g/cm³) and a relatively high Nct (3875). Again, this indicates an association of atoms of high atomic number with alteration minerals.

F5. X-ray CT images of whole-round core samples, p. 11.

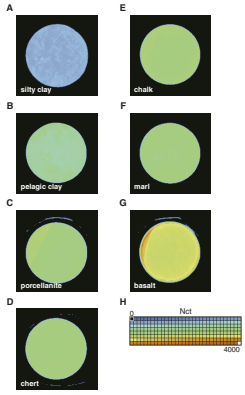

F6. Three-dimensional X-ray CT image of a whole-round core sample, p. 12.

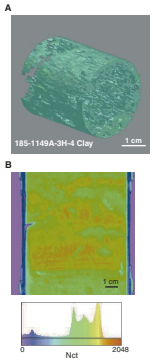

F7. X-ray CT images of selected cube samples, p. 13.

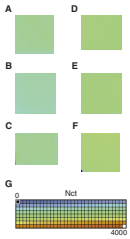

F8. Crossplot of average Ncts from all cube samples, p. 14.

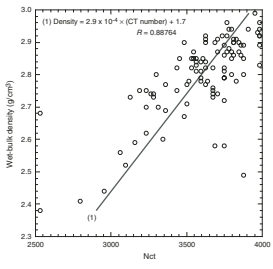

ACKNOWLEDGMENTS

This research used samples and data provided by the Ocean Drilling Program (ODP). ODP is sponsored by the U.S. National Science Foundation and participating countries under the management of the Joint Oceanographic Institutions, Inc. This project was partially funded by a U.S. Science Support Program grant to the second author and Center for Marine Science Contribution #256.

We are grateful to ODP for inviting our participation on Leg 185, to all members of the Shipboard Scientific Party of Leg 185 for their cooperation on board the ship, and to the ODP personnel and the Sedco crew who made Leg 185 a success. The first author is grateful to Dr. Yoshito Nakashima (Geological Survey of Japan, AIST, Japan) for providing X-ray CT imaging equipment.

REFERENCES

Hounsfield, G.N., 1973. Computerized transverse axial scanning (tomography), Part I. Description of system. *Br. J. Radiol.,* 46:1016–1022.

Shipboard Scientific Party, 2000a. Site 801. *In* Plank, T., Ludden, J.N., Escutia, C., et al., *Proc. ODP, Init. Repts.,* 185, 1–222 [CD-ROM]. Available from: Ocean Drilling Program, Texas A&M University, College Station TX 77845-9547, USA.

————, 2000b. Explanatory notes. *In* Plank, T., Ludden, J.N., Escutia, C., et al., *Proc. ODP, Init. Repts.,* 185, 1–76 [CD-ROM]. Available from: Ocean Drilling Program, Texas A&M University, College Station TX 77845-9547, USA.

Figure F1. Schematic diagram for sampling. Cube samples were used for shipboard measurements of *P*-wave velocity and shore-based measurements of electrical resistivity and X-ray CT. Shipboard measurements of moisture and density were made on samples adjacent to cut cubes.

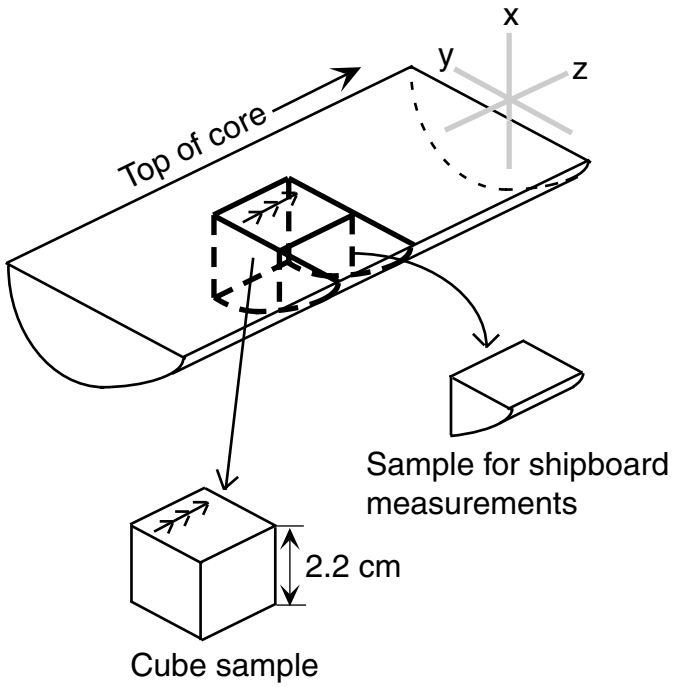

Figure F2. **A**. Schematic diagram of the equipment used for measuring electrical resistivity. **B**. Photograph of the apparatus with a sample cube.

A

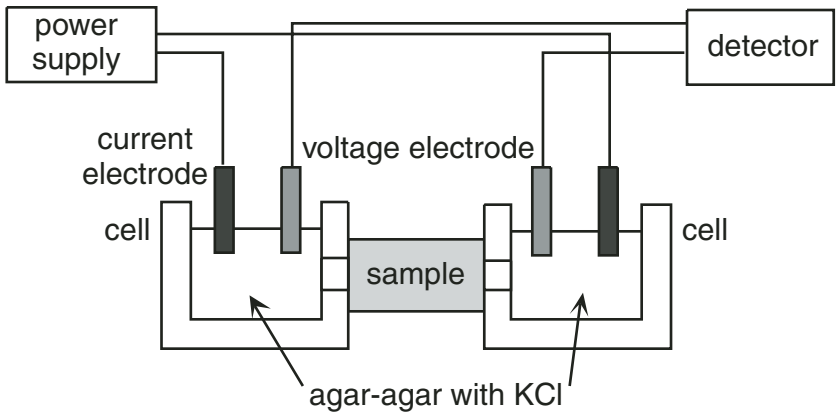

B

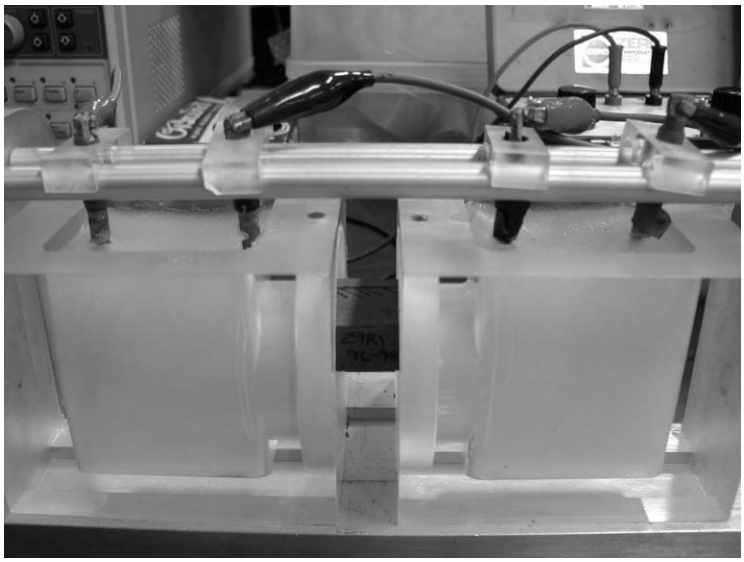

Figure F3. Wet resistivities along three mutually perpendicular directions from cube samples from Hole 801C. Downhole measurements of borehole resistivity from the Dual Laterolog tool are plotted as a solid line. Circles = x-direction, diamonds = y-direction, crosses = z-direction.

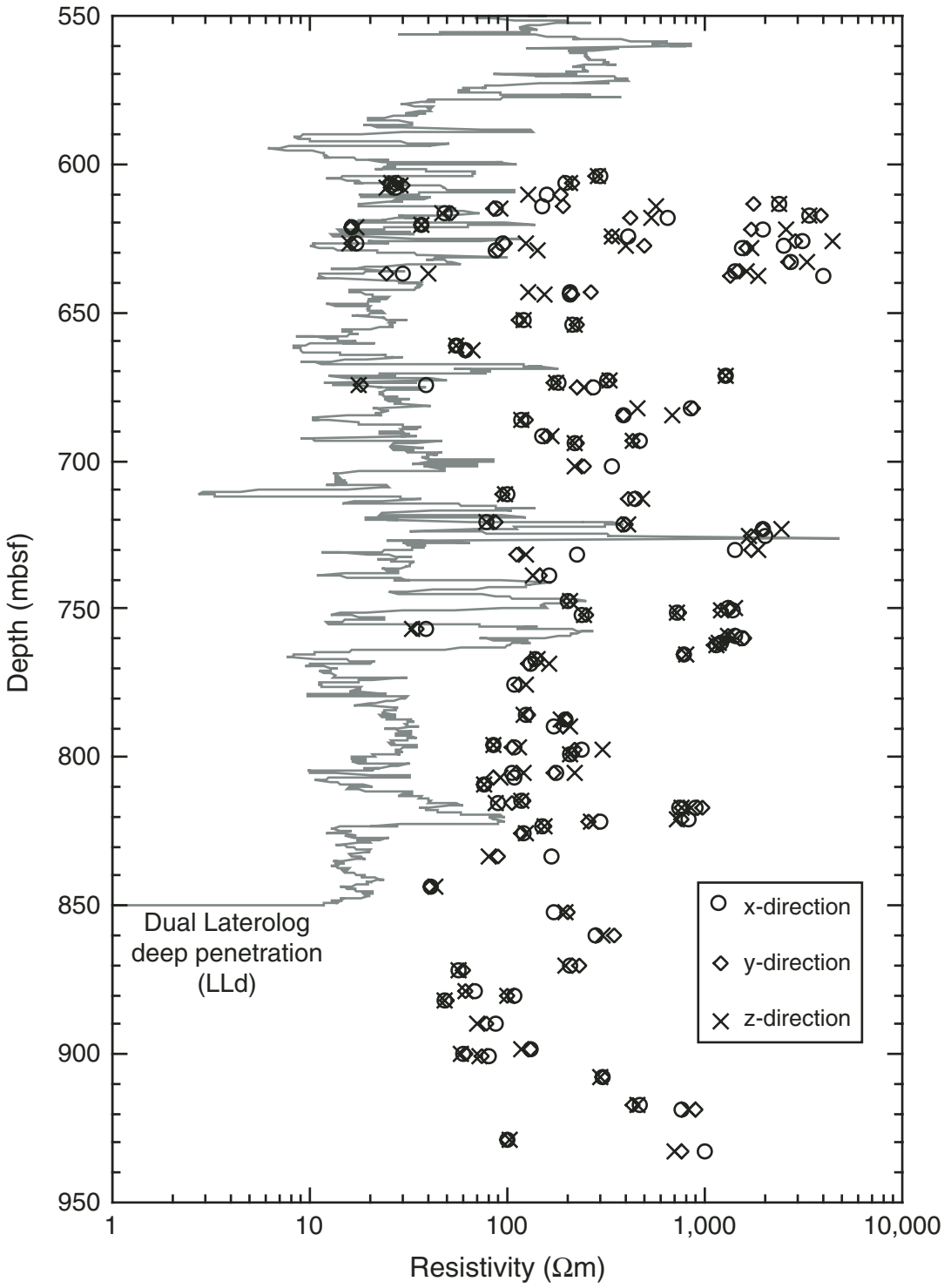

Figure F4. **A**. Photograph of the medical X-ray CT scanner W2000. **B**. Schematic of slice imaging of an X-ray CT. **C**. Thickness of each slice = 1 mm.

A

B

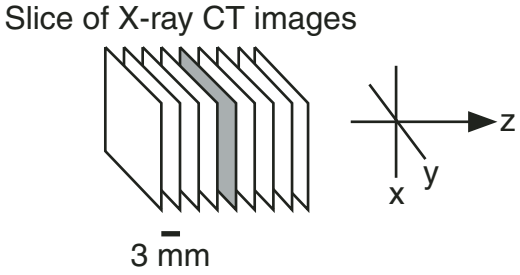

C

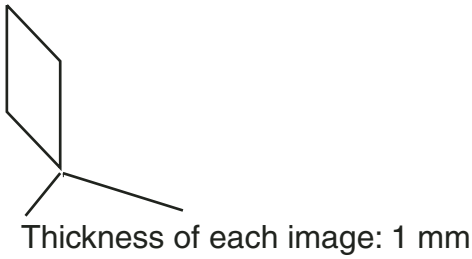

Figure F5. X-ray CT images of whole-round core samples from Site 1149. **A**. Sample 185-1149A-3H-4, 130–140 cm. **B**. Sample 185-1149A-17H-2, 140–150 cm. **C**. Sample 185-1149C-6R-1, 47–53 cm. **D**. Sample 185-1149B-18R-1, 121–126 cm. **E**. Sample 185-1149B-27R-1, 0–12 cm. **F**. Sample 185-1149C-8R-1, 47–51 cm. **G**. Sample 185-1149D-8R-1, 83–90 cm. **H**. Color scale for the Nct. Each color grade has a range of 15.625 Nct. Blue = low attenuation, red = high attenuation. Lithologies are as given during Leg 185 (Shipboard Scientific Party, 2000a). Nct = CT number.

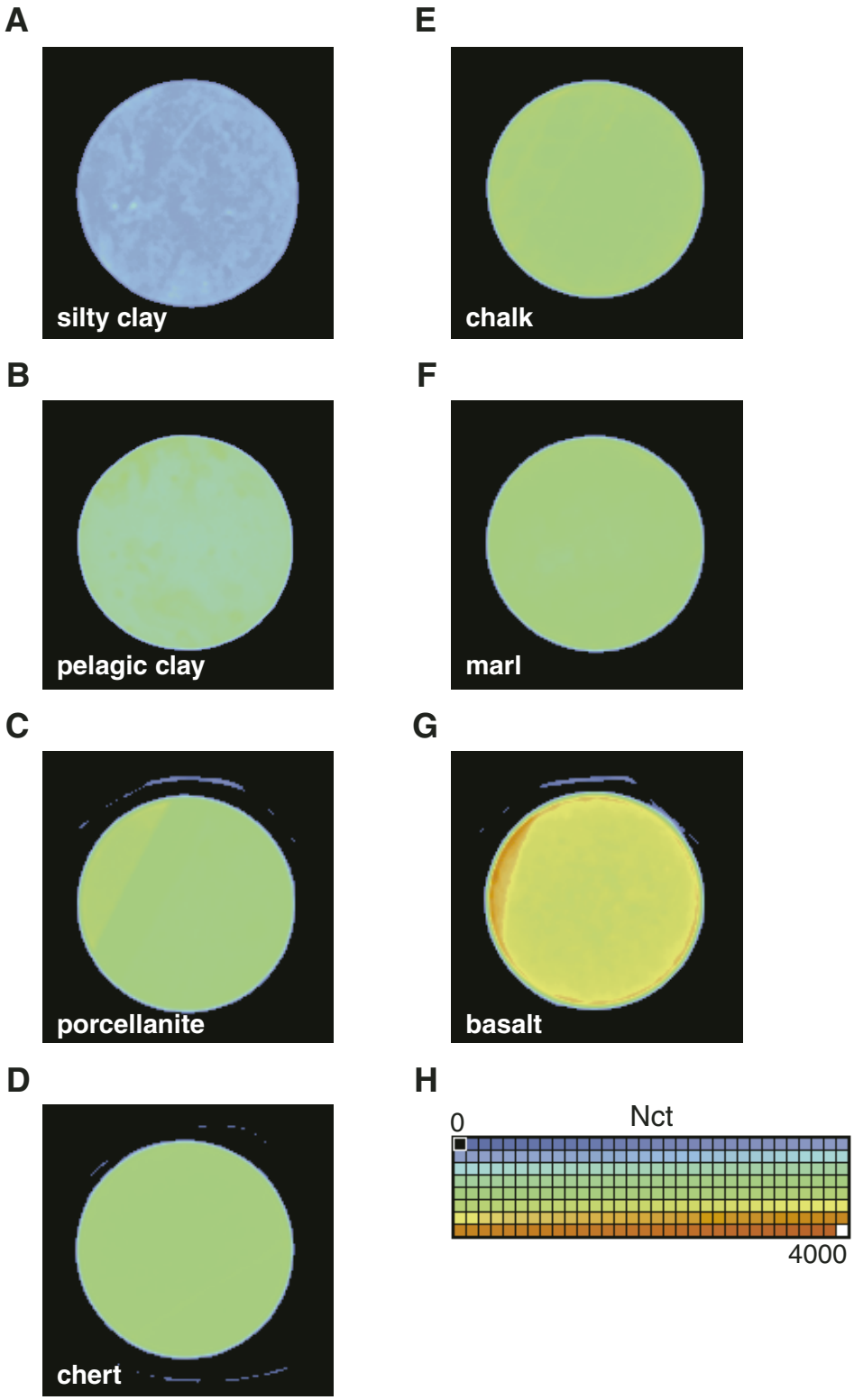

Figure F6. **A**. Three-dimensional X-ray CT image of a whole-round clay sample (Sample 185-1149A-3H-4, 130–140 cm). **B**. Vertical (z) cross section of the sample with CT number (Nct) color scale. Blue = low attenuation, red = high attenuation.

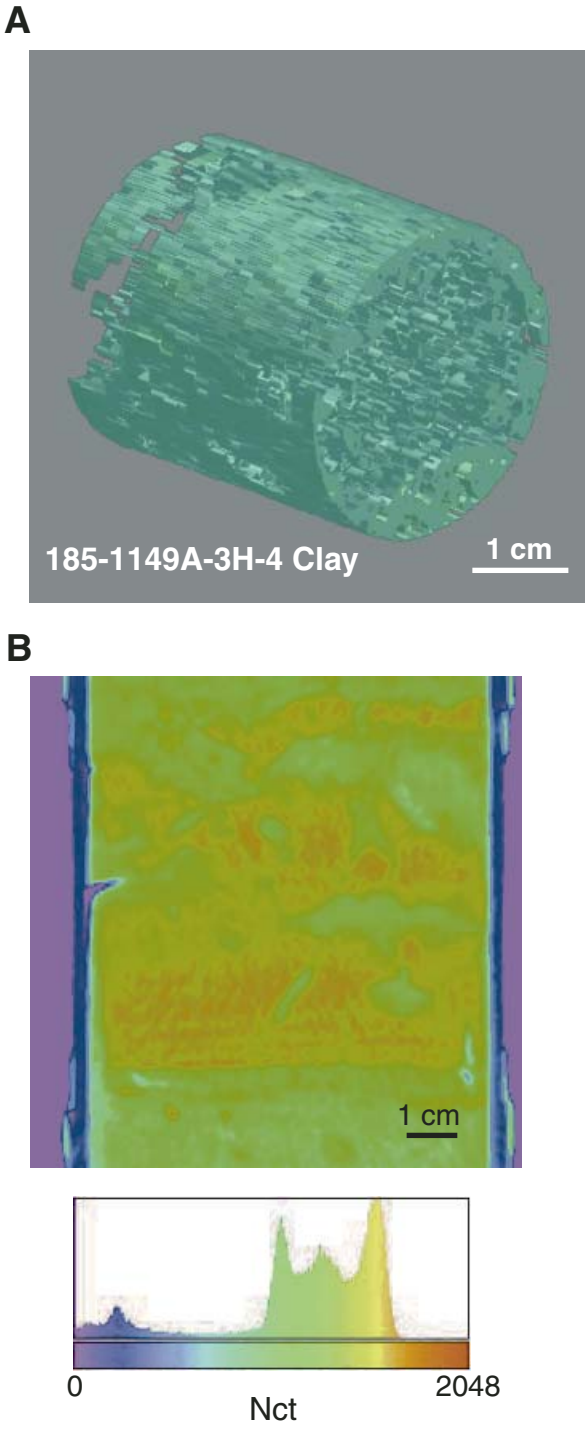

Figure F7. X-ray CT images of selected cube samples recovered from Hole 1149B. **A**. Sample 185-1149B-7R-1, 3–5 cm. **B**. Sample 185-1149B-16R-1, 79–81 cm. **C**. Sample 185-1149B-18R-1, 15–17cm. **D**. Sample 185-1149B-24R-1, 31–33 cm. **E**. Sample 185-1149B-27R-1, 14–16 cm. **F**. Sample 185-1149B-28R-2, 36–38 cm. **G**. Color scale for CT number (Nct). Each color grade has a range of 15.625 Nct. Blue = low attenuation, red = high attenuation.

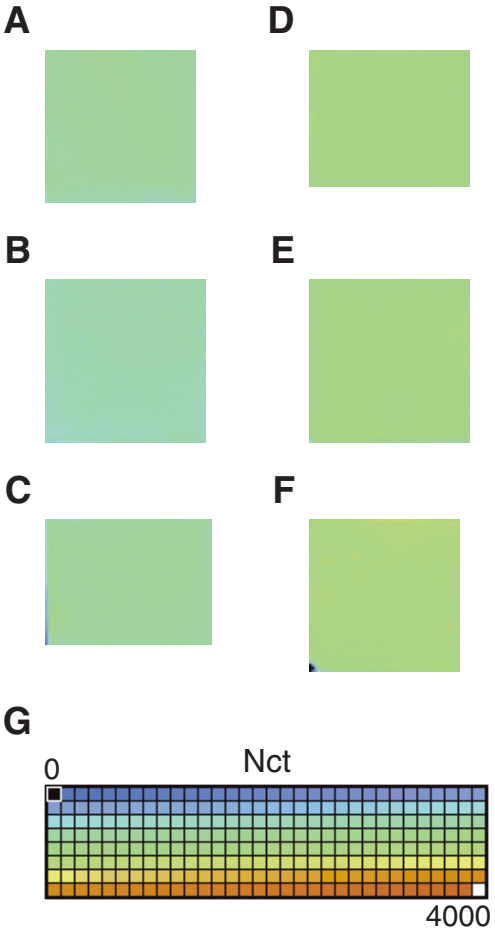

Figure F8. Crossplot of average CT numbers (Ncts) from all cube samples (see Tables T1, p. 15; T2, p. 17) and shipboard wet bulk density (Shipboard Scientific Party, 2000a; see Table T11, p. 204, in the "Site 801" chapter). One different least-squares regression line is shown in this graph.

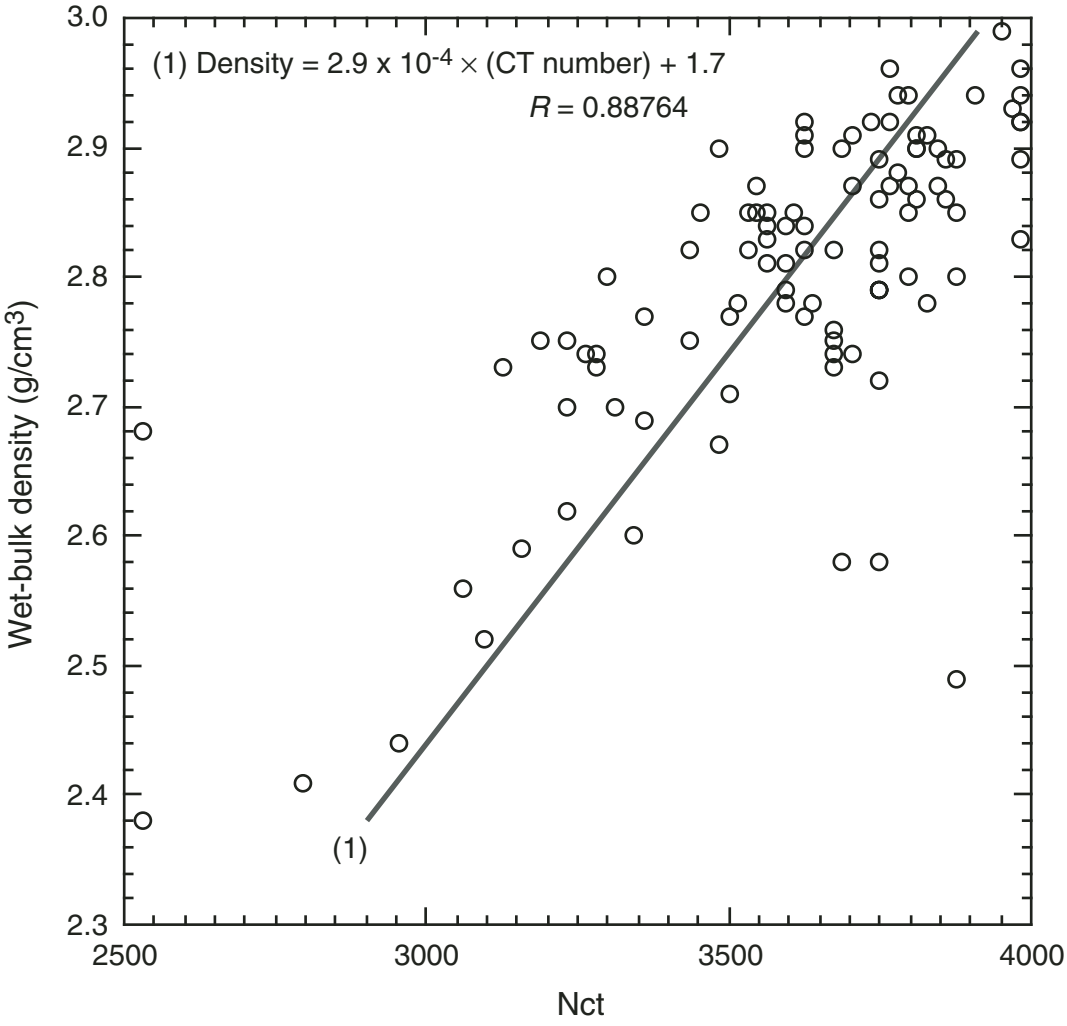

Table T1. Wet and dry resistivity along three orthogonal directions and average Nct of cube sample, Hole 801C. (Continued on next page.)

Core, section, interval (cm)	Depth (mbsf)	Resistivity (Ωm)						Average Nct	Lithology	Igneous structure	Igneous unit
		x (dry)	y (dry)	z (dry)	x (wet)	y (wet)	z (wet)				
185-801C-											
14R-1, 38–40	604.38	282.9	304.3	289.1	294.4	279.6	287.8	3562.5	Aphyric basalt	Flow	34
14R-2, 81–83	606.12	22.1	22.5	21.5	27.0	25.5	25.6	3093.8	Aphyric basalt	Flow	34
14R-2, 121–123	606.52	152.7	166.4	166.9	199.8	214.4	209.4	3437.5	Aphyric basalt	Pillow	35
14R-3, 44–46	607.22	20.8	24.8	25.2	25.7	29.8	28.9	3062.5	Aphyric basalt	Pillow/flow	37–2
14R-3, 96–98	607.74	20.7	19.4	18.9	27.0	26.0	24.3	3750.0	Interpillow material (orange)	Pillow	37–5
14R-5, 51–53	610.13	181.1	220.2	124.1	159.3	186.5	128.7	3671.9	Aphyric basalt	Pillow/flow	38–4
15R-1, 12–14	613.82	9999.9	9999.9	9999.9	2371.8	1771.3	2372.5	3265.6	Interpillow material (white/ green)	Breccia	39
15R-1, 72–74	614.42	101.2	111.0	288.0	151.4	193.3	563.9	3984.4	Interpillow sediment (red)	Sediment	40
15R-2, 9–11	615.11	85.5	84.4	94.9	86.6	85.9	92.3	3484.4	Aphyric basalt	Pillow	41–3
15R-3, 50–52	616.91	44.8	47.2	44.1	48.7	52.2	47.3	3234.4	Aphyric basalt	Pillow	43–5
15R-3, 118–120	617.59	9999.9	9999.9	9999.9	3380.4	3847.6	3379.3	3625.0	Interpillow material (red/ brown)	Sediment	43–8
15R-4, 60–62	618.31	524.3	378.7	496.1	652.8	416.5	541.7	3562.5	Aphyric basalt	Flow	44
15R-6, 14–16	620.12	34.0	33.8	34.3	37.3	36.9	36.7	3234.4	Aphyric basalt	Flow	45
15R-7, 13–15	621.51	11.1	11.7	12.6	16.3	16.2	17.2	2531.3	Aphyric basalt (pale green)	Pillow	46–2
15R-7, 51–53	621.89	9999.9	9999.9	9999.9	1953.4	1713.7	2576.6	3187.5	Interpillow material (brownish red)	sediment	46–3
16R-1, 89–91	624.19	335.9	315.2	314.0	404.8	339.0	339.7	3765.6	Aphyric basalt	Pillow	47–3
16R-3, 8–10	626.1	NR	NR	NR	3112.1	2869.5	4487.1	3156.3	Hydrothermal deposit (yellow)	Hydrothermal	48
16R-3, 45–47	626.47	71.4	74.0	83.5	94.6	96.5	123.7	3843.8	Interpillow material	Sediment	49–1
16R-3, 85–87	626.87	27.0	19.6	12.4	17.1	16.3	15.9	2796.9	Aphyric basalt (green)	Pillow	49–2
16R-4, 1–3	627.44	NR	593.2	545.0	2506.6	496.2	393.6	3812.5	Aphyric basalt	Flow	49–3
16R-4, 72–74	628.15	9999.9	9999.9	9999.9	1551.4	1647.8	1701.4	3625.0	Aphyric basalt	Flow	49–3
16R-5, 49–51	629.38	85.1	76.0	125.5	86.4	90.7	142.7	3593.8	Aphyric basalt	Pillow	49–5
17R-1, 50–52	633.3	9999.9	9999.9	9999.9	2728.4	2670.1	3302.0	3796.9	Aphyric basalt	Pillow	49–7
17R-3, 37–39	636.15	9999.9	9999.9	9999.9	1436.9	1483.3	1621.5	3875.0	Aphyric basalt	Pillow	49–11
17R-3, 121–123	636.99	29.6	19.9	39.2	29.9	24.3	40.4	3343.8	Aphyric basalt	Pillow	49–13
17R-4, 88–90	638.1	9999.9	9999.9	9999.9	4021.9	1366.9	1850.1	2531.3	Interpillow material (white/ green)	Pillow	50–5
18R-1, 79–81	642.99	224.2	294.6	146.3	208.1	265.0	127.6	3828.1	Aphyric basalt	Pillow	50–8
18R-2, 30–32	644	207.6	168.2	136.0	209.4	213.6	155.4	3671.9	Aphyric basalt	Pillow	50–10
19R-1, 71–73	652.41	114.6	109.3	120.8	120.8	113.7	121.1	3703.1	Aphyric basalt	Flow	50–14
19R-3, 6–8	654.45	235.6	222.1	238.2	213.1	223.0	220.9	3609.4	aphyric basalt	Flow	50–18
20R-1, 45–47	661.15	47.5	50.9	51.6	55.1	54.8	55.2	3750.0	aphyric basalt	Flow	50–21
20R-2, 94–96	663.06	57.6	58.6	61.6	61.1	61.6	67.0	3359.4	aphyric basalt	Flow	50–24
21R-1, 100–102	671	1369.6	1327.9	1319.2	1262.2	1270.9	1277.8	3828.1	aphyric basalt	Pillow/flow	50–26
21R-2, 117–119	672.6	398.5	334.3	330.9	322.1	326.3	331.4	3671.9	aphyric basalt	Pillow/flow	50–27
21R-3, 70–72	673.35	202.5	165.3	174.6	182.8	170.4	178.1	3500.0	aphyric basalt	Pillow/flow	50–27
22R-1, 114–116	674.74	48.7	18.2	16.7	39.3	17.9	17.6	2953.1	Aphyric basalt with vein	Pillow/flow	50–36
22R-2, 60–62	675.44	221.5	227.7	250.5	272.1	224.6	246.9	3625.0	Aphyric basalt	Flow	50–39
23R-1, 39–41	682.29	822.4	910.3	490.1	844.7	876.8	457.4	3812.5	Aphyric basalt	Flow	50–43
23R-3, 41–43	684.99	378.1	399.1	652.4	385.1	386.1	694.0	3781.3	Aphyric basalt	Flow	50–45
23R-4, 58–60	686.56	119.6	126.6	117.4	119.1	122.9	117.5	3593.8	Aphyric basalt	Pillow/flow	50–48
24R-1, 35–37	691.65	149.4	215.5	167.3	150.0	160.1	168.5	3593.8	Aphyric basalt	Pillow/flow	50–51
24R-2, 44–46	693.07	518.4	393.9	389.9	465.5	432.6	431.7	3859.4	Aphyric basalt	Flow	50–55
24R-3, 22–24	694.35	237.9	244.9	236.7	222.6	224.3	217.0	3796.9	Aphyric basalt	Pillow	50–57
25R-1, 95–97	701.65	362.3	249.2	229.8	336.5	246.8	220.5	3812.5	Aphyric basalt	Pillow	50–61
26R-1, 96–98	711.16	120.0	94.6	93.1	99.2	95.7	97.1	3796.9	Aphyric basalt	Flow	50–65
26R-2, 100–102	712.53	409.7	401.3	493.7	438.7	413.2	479.7	3875.0	Aphyric basalt	Flow	50–65
27R-1, 98–100	720.68	107.0	80.4	81.1	77.6	86.6	79.6	3531.3	Aphyric basalt	Flow	50–68
27R-2, 39–41	721.37	516.1	450.0	490.7	385.2	399.6	410.6	3781.3	Aphyric basalt	Flow	50–69
27R-3, 84–86	723.32	9999.9	9999.9	9999.9	1962.2	1956.4	2452.1	3703.1	Aphyric basalt	Flow	50–71
27R-4, 141–143	725.19	9999.9	9999.9	9999.9	2052.2	1734.4	1692.7	3703.1	Aphyric basalt	Flow	50–71
28R-2, 22–24	730.26	9999.9	9999.9	9999.9	1436.9	1743.8	1869.0	3734.4	Aphyric basalt	Flow	50–72
28R-2, 144-146	731.48	258.6	108.4	133.2	225.5	111.2	125.8	3984.4	T. Hirono, personal sample		
29R-1, 96–98	738.86	173.5	152.3	150.0	161.2	147.2	136.8	3625.0	Sparsely olivine phyric basalt	Flow	51–2
30R-1, 19–21	747.49	278.1	231.0	237.4	204.7	210.2	209.1	3593.8	Sparsely olivine phyric basalt	Flow	51–2
30R-2, 101–103	749.75	1658.5	1603.4	1547.9	1315.2	1351.4	1416.4	3843.8	Sparsely olivine phyric basalt	Flow	51–2
30R-3, 67–69	750.73	1555.6	1267.8	1283.1	1399.7	1211.3	1206.2	3703.1	Sparsely olivine phyric basalt	Flow	51–2
30R-4, 5–7	751.43	878.9	808.4	851.2	732.3	738.2	716.2	3859.4	Sparsely olivine phyric basalt	Flow	51–2
30R-5, 12–14	752.28	312.7	283.0	289.6	241.6	249.5	246.1	3750.0	Sparsely olivine phyric basalt	Flow	51–3
31R-1, 40–42	757	60.9	43.3	40.8	39.2	34.5	33.1	3359.4	Sparsely olivine phyric basalt	Flow	51–5
31R-2, 86–88	758.76	1650.3	1518.7	2025.9	1428.1	1317.9	1330.7	3953.1	Sparsely olivine phyric basalt	Flow	51–6
31R-3, 50–52	759.68	2459.1	2458.9	2379.4	1529.5	1570.4	1399.5	3984.4	Sparsely olivine phyric basalt	Flow	51–6
31R-4, 52–54	761.11	1475.9	1432.5	1491.8	1204.1	1170.0	1165.4	3765.6	Sparsely olivine phyric basalt	Flow	51–6
31R-5, 1–3	762.05	1682.5	1292.1	1392.1	1160.8	1127.6	1141.9	3968.8	Sparsely olivine phyric basalt	Flow	51–6

Table T1 (continued).

Core, section, interval (cm)	Depth (mbsf)	Resistivity (Ωm)						Average Nct	Lithology	Igneous structure	Igneous unit
		x (dry)	y (dry)	z (dry)	x (wet)	y (wet)	z (wet)				
31R-7, 93–95	765.67	920.2	918.9	1019.8	786.4	787.6	807.1	3812.5	Sparsely olivine phyric basalt	Flow	51–6
32R-1, 25–27	766.55	155.0	160.0	155.2	138.8	142.4	142.8	3875.0	Sparsely olivine phyric basalt	Flow	51–6
32R-2, 57–59	768.37	154.8	156.7	171.1	131.0	127.4	161.9	3687.5	Aphyric basalt	Pillow/flow	52–4
33R-1, 11–13	775.81	166.5	151.8	171.0	109.3	113.9	124.4	3875.0	Aphyric basalt	Pillow/flow	52–4
34R-1, 48–50	785.78	166.3	158.9	164.3	124.5	127.5	122.8	3656.3	Sparsely olivine phyric basalt	Pillow/flow	53–2
34R-2, 61–63	787.15	220.3	192.4	187.8	198.2	195.1	186.4	3687.5	Sparsely olivine phyric basalt	Pillow/flow	53–3
34R-3, 129–131	789.3	244.4	224.6	262.4	173.8	191.2	206.1	3984.4	Sparsely olivine phyric basalt	Flow	53–7
35R-1, 84–86	795.74	84.6	90.1	87.4	84.8	84.4	86.2	3671.9	Sparsely olivine phyric basalt	Flow	53–8
35R-2, 4–6	796.31	135.3	136.8	145.6	108.6	105.1	115.8	3984.4	Sparsely olivine phyric basalt	Flow	53–8
35R-2, 122–124	797.49	257.4	213.1	297.4	236.9	219.6	304.2	3671.9	Sparsely olivine phyric basalt	Pillow/flow	53–9
35R-4, 9–11	799.21	270.6	272.7	297.2	206.0	215.3	209.7	3984.4	Sparsely olivine phyric basalt	Flow	53–12
36R-1, 113–115	805.23	142.1	141.6	150.7	106.6	112.9	119.6	3796.9	Aphyric basalt	Flow	53–14
36R-2, 11–13	805.55	205.7	192.5	242.4	177.1	173.0	219.3	3750.0	Aphyric basalt	Pillow	53–15
36R-3, 41–43	807.18	131.4	104.6	103.3	109.3	84.2	91.3	3640.6	Aphyric basalt	Flow	53–16
36R-4, 106–108	809.25	113.7	80.7	84.0	77.1	77.1	76.6	3750.0	Aphyric basalt	Flow	53–19
37R-1, 140–142	814.7	122.3	131.1	124.5	117.6	121.9	116.9	3453.1	Aphyric basalt	Flow	54
37R-2, 42–44	815.17	94.0	108.4	93.6	89.8	105.1	86.5	3750.0	Aphyric basalt	Flow	54
37R-3, 117–119	117.02	951.9	997.7	946.9	734.8	760.6	761.7	3625.0	Aphyric basalt	Flow	54
37R-4, 8–10	817.34	1375.0	1282.1	1344.1	890.5	965.4	848.0	3984.4	Aphyric basalt	Flow	54
37R-6, 72–74	820.52	1407.2	943.2	1103.5	838.2	769.9	727.7	3546.9	Aphyric basalt	Flow	54
37R-7, 68–70	821.98	397.1	311.5	332.0	293.4	262.1	263.5	3546.9	Aphyric basalt	Flow	54
38R-1, 35–37	823.15	153.7	164.5	161.6	149.6	153.9	153.6	3484.4	Aphyric basalt	Flow	54
38R-2, 113–116	825.39	194.9	160.7	155.8	120.5	118.1	123.6	3890.6	Aphyric basalt	Flow	54
39R-1, 104–106	833.24	271.7	127.6	107.1	165.8	89.4	81.7	3750.0	Aphyric basalt	Flow	55–6
40R-2, 68–70	843.66	57.3	46.2	48.1	41.1	41.1	43.6	3234.4	Aphyric basalt breccia	Breccia	56
41R-1, 109–111	851.89	263.0	221.9	249.4	174.2	205.1	197.3	3562.5	Aphyric basalt	Flow	57
42R-1, 32–33	860.32	439.8	463.6	516.4	282.6	348.2	301.7	3625.0	Aphyric basalt	Flow	57
43R-1, 99–101	870.09	289.7	310.6	279.0	207.8	231.0	197.4	3750.0	Aphyric basalt	Pillow	58–3
43R-2, 112–114	871.68	75.3	79.2	83.2	56.2	60.0	57.0	3500.0	Aphyric basalt	Flow	58–3
44R-1, 18–20	878.98	69.4	70.9	71.8	69.3	61.6	62.0	3296.9	Aphyric basalt	Flow	59
44R-2, 62–64	880.68	144.0	136.4	145.0	109.0	99.9	100.7	3562.5	Aphyric basalt	Flow	59
44R-3, 32–34	881.88	60.6	62.5	55.4	48.1	50.1	48.1	3281.3	Aphyric basalt	Flow	59
45R-2, 34–36	890.1	125.9	99.1	90.8	87.6	78.4	71.0	3281.3	Aphyric basalt	Pillow/flow	60–4
46R-1, 19–21	898.19	161.2	184.1	169.1	130.3	131.0	117.5	3531.3	Aphyric basalt	Flow	60–7
46R-2, 90–92	900.32	70.9	69.5	70.7	60.2	61.2	58.3	3125.0	Aphyric basalt	Flow	60–7
46R-3, 36–38	901.07	106.8	79.4	81.3	80.9	74.8	73.0	3312.5	Aphyric basalt	Pillow/flow	60–8
47R-1, 29–35	907.99	397.6	296.7	293.2	300.4	307.7	299.2	3437.5	Aphyric basalt	Pillow	60–11
48R-1, 49–51	917.19	562.7	515.7	554.7	463.4	436.2	460.9	3906.3	Aphyric basalt	Pillow/flow	60–13
48R-2, 98–100	918.98	897.3	1102.8	966.8	758.8	907.7	825.6	3328.1	Aphyric basalt	Pillow/flow	60–15
49M-1, 43–45	928.73	105.8	99.0	103.1	100.7	100.9	103.2	3515.6	Aphyric basalt	Pillow	60–18
52M-1, 8–10	932.88	1041.3	828.4	411.0	1009.8	759.7	704.4	3765.6	Aphyric basalt	Pillow/flow	60–26

Notes: Nct = CT number. NR = no recovery.

Table T2. Wet and dry resistivity along three orthogonal directions of cube samples, Site 1149.

Core, section, interval (cm)	Depth (mbsf)	Resistivity (Ωm)						Average Nct	Lithologic unit
		x (dry)	y (dry)	z (dry)	x (wet)	y (wet)	z (wet)		
7R-1, 3–5	203.73	29.8	31.5	25.2	27.6	26.5	24.0	1516	Unit III (porcellanite)
16R-1, 79–81	283.09	13.7	12.6	12.3	11.3	11.9	11.1	1093	Unit IV (chalk)
18R-1, 15–17	301.75	17.8	11.8	15.2	12.8	9.7	10.3	1250	Unit IV (marl)
24R-1, 31–33	359.51	233.3	231.8	347.6	159.9	153.9	244.3	1875	Unit IV (chert)
27R-1, 14–16	387.74	21.7	16.8	26.3	13.2	12.1	14.6	2234	Unit IV (marl)
28R-2, 36–38	398.78	20.2	14.5	24.3	13.5	14.5	17.2	2500	Unit IV (marl)

Notes: Lithology and lithologic units are as defined during Leg 185 (Shipboard Scientific Party, 2000a). Nct = CT number.

Table T3. Index properties, resistivity, and Nct number of whole-round core samples, Site 1149.

Core, section	Depth (mbsf)	Wet-bulk density (g/cm^3)	Porosity (%)	Void ratio	Water content (%)	Resistivity (Ωm)	*P*-wave velocity (m/s)	Average Nct	Lithology
185-1149A-									
3H-4	19.50	1.46	72.9	2.69	51.2	68.65	1532	696	Clay (Unit I)
8H-4	67.10	1.43	74.8	2.97	53.5	73.83	1515	832	Clay (Unit I)
13H-4	114.60	1.33	80.9	4.24	62.5	33.66	1554	640	Clay (Unit I)
17H-2	149.60	1.36	60.8	1.55	45.7	32.2	1522	944	Clay (Unit II)
185-1149B-									
3R-1	171.70	1.50	70.8	2.43	48.5	49.68	1508	1328	Clay (Unit II)
18R-1	302.81	2.33	5.1	0.05	2.2	3665.33	4946	2000	Chert
27R-1	387.60	2.21	32.9	0.49	15.2	80.47	2172	2016	Chalk
29R-3	410.58	2.69	6.4	0.07	2.5	632.7	4606	2781	Basalt
30R-2	418.33	2.59	9.0	0.10	3.5	355.93	4840	2641	Basalt
185-1149C-									
6R-1	312.87	2.19	8.0	0.09	3.7	3491.46	3219	1797	Porcellanite
8R-1	388.67	2.37	24.7	0.33	10.7	135.65	2356	1828	Marl
11R-1	418.41	2.31	8.1	0.09	3.6	459.77	5167	2016	Basalt
185-1149D-									
8R-1	330.13	2.77	5.9	0.06	2.2	427.46	4569	1828	Basalt

Notes: Shore-based moisture and density were measured using equipment and methods similar to those used during Leg 185 (Shipboard Scientific Party, 2000b). Lithology and lithologic units are as defined during Leg 185 (Shipboard Scientific Party, 2000a). Nct = CT number.